Cement and Concrete Research 48 (2013) 1–8

Contents lists available at SciVerse ScienceDirect

Cement and Concrete Research

journal homepage: http://ees.elsevier.com/CEMCON/default.asp

Investigation of different fracture modes in cement-based materials by acoustic emission

D.G. Aggelis [a,*], A.C. Mpalaskas [b], T.E. Matikas [b]

[a] Department of Mechanics of Materials and Constructions, Vrije Universiteit Brussel, Pleinlaan 2, 1050 Brussels, Belgium
[b] Department of Materials Science and Engineering, University of Ioannina, 45110 Ioannina, Greece

ARTICLE INFO

Article history:
Received 27 April 2012
Accepted 12 February 2013
Available online xxxx

Keywords:
Acoustic emission
Characterization (B)
Mortar (E)
Finite Element Analysis (C)
Crack Detection (B)

ABSTRACT

Characterization of the cracking mode in cementitious materials allows evaluations concerning the remaining life of the structure since in general, shear-like phenomena occur after tensile cracking. Individual modes of cracking cause different motion of the crack tip dictating the waveforms emitted after cracking events. In this study fracture experiments on cementitious specimens are conducted. The fracture mode is controlled by modifying the experiment geometry and the process is monitored by acoustic emission. The distinct signature of the cracking modes is reflected on acoustic waveform parameters like the amplitude, RA-value and frequency. Signals emitted by the shear testing exhibit longer waveforms and lower frequency than those by the tensile testing. The influence of inhomogeneity is also evident as signals acquired at different distances exhibit distinct characteristics. Results show that AE study leads to characterization of the dominant fracture mode using only two AE descriptors and offers the potential for in-situ application.

1. Introduction

Characterization of the fracture mode in engineering materials is a task concentrating a lot of effort in the engineering community. This is particularly important since during the fracture process, a sequence of fracturing modes is generally followed. Therefore, characterization of the dominant mode highlights the stage of failure (initial, intermediate or final). Specifically for concrete, a lot of work has been done showing that shear phenomena dominate at the last stages of failure, while initially, tensile mode is mostly active [1–5]. A method that is suitable for the monitoring of the fracture phenomena is acoustic emission (AE). AE gives the opportunity to highlight the moments of major or minor fracture occurrences and follows the procedure until final failure. Information of the population of the AE signals, as well as specific indices enlighten the understanding of the fracture process and enable the evaluation of the general condition of the material each moment. Concerning the fracture mode characterization, moment tensor analysis (MTA) has been developed and successfully applied in laboratory experiments [6]. The fracture mode is evaluated and reasonably correlated with the observation of the location of the cracks after failure [1,6]. However, the use of MTA is not easy in real structures due to practical limitations. The most important is that each AE event needs to be recorded by as many as eight individual sensors in order to supply enough information on the directionality of the acoustic wave. In large structures the sensors are distributed in relatively long distances in order to cover as much volume of the structure as possible and enable evaluations on the whole scale. Therefore, when using sensor separation distances of several meters [7,8] it is highly unlikely to record the transient waves of the same event with the required number of sensors due to inherent material attenuation. In light of the above, a reliable characterization scheme that requires less number of sensors is desirable which however, can provide useful and reliable information on the material's damage status.

The problem of accurate characterization of the cracking condition in a material is a nearly impossible task. In order to fully describe the damage condition within a material, several parameters should be evaluated. These include the size, shape and orientation of each crack, the fracture mode under which it propagates as well as its propagation rate under a specific loading pattern. Considering that any large concrete structure includes numerous cracks either from construction or function loads, one realizes that successfully dealing with the problem of damage status characterization in its absolute form is highly unlikely. Still, information on the general condition is vital. If this information derived by NDT monitoring is the basis for a maintenance procedure that potentially extends the safe service life for decades, it is understood that even rough evaluations attain great significance. Additionally, indices obtained as a function of time enable comparisons between the behavior and performance of the structure before and after sustaining additional loading. An effort has been undertaken in order to monitor damage of cementitious materials based on the recording of simple AE parameters. A description of AE monitoring and the main signal descriptors follows.

AE allows monitoring of crack growth using transducers placed on the material. These transducers record the transient response of the

* Corresponding author: Tel.: +32 2 629 3541; fax: +32 2 6292928.
E-mail address: daggelis@vub.ac.be (D.G. Aggelis).

0008-8846/$ – see front matter © 2013 Elsevier Ltd. All rights reserved.
http://dx.doi.org/10.1016/j.cemconres.2013.02.002

surface after each cracking event (similar to seismic activity) and transform it into electrical voltage due to their piezoelectric nature [9]. The information that can be drawn concerns the cracks' location and the total activity, which is related to the number and the nature of cracking events [10,11]. Detailed study of qualitative parameters of the received waveforms leads to characterization of the fracture process [1–6] and sustained damage assessment [10,12,13]. Certain AE features have been successfully correlated to the fracture process. One is the maximum amplitude (A) of the waveform that depends on the intensity of the cracking source, see Fig. 1a. Another important descriptor is "RA value" which is the duration of the first, rising part of the waveform (rise time, RT) over A measured in μs/V, and has been shown to be very sensitive to the fracture mode [4,14,15]. Frequency parameters like the "average frequency", AF, are also important. AF is the number of threshold crossings over the duration of the signal, measured in kHz. Another important frequency feature is the peak frequency, PF, which is the frequency with the maximum magnitude after fast Fourier transformation of the waveform [16], see Fig. 1b. The individual modes of failure lead to wave emissions with different characteristics allowing characterization of cracks based on their mode [17]. Several studies have shown that tensile cracks lead to AE with higher frequency characteristics and lower RA values than shear cracks [1–4,14,15]. Apart from damage, AE parameters have also been used to highlight other processes like self-healing in concrete [18,19], melting of particles in a matrix [20] or correlating with strength and particle/inclusion size [11,21].

In most of the above works tensile and shear phenomena are successfully distinguished by their AE behavior. However, the distinct fracture signatures are exhibited by various kinds of phenomena and not by the different fracture modes of the material itself. As an example, in steel fiber reinforced concrete [3,4] under bending, tensile cracks are related to matrix cracking. On the other hand shear phenomena are associated with fiber-pull out. The first depends on the strength and quality of the concrete matrix, while the second on the interfacial shear strength between the matrix and the fibers. Similarly matrix cracking and delaminations are monitored in laminated composites [11,22,23]. The first is basically associated to the tensile strength of the off-axis layers, while delaminations depend again on the interfacial shear strength between successive layers. In the present paper the modes of fracture are associated with the core material itself (cement based matrix), without other sources of inhomogeneity like fibers or laminas. The geometry of the testing experiment was slightly modified in order to excite different fracture modes as expressed by the dominant normal or shear stresses developed at the position of cracking as also suggested by finite element simulation. The material was a cementitious mortar with small aggregates (sand) which is considered relatively homogeneous to concrete that includes large aggregates. AE was monitored during fracture and the differences between the typical signals received during shear and tension are highlighted. It is seen that, at least in laboratory conditions, characterization of fracture mode can be reliably conducted based on the results of just one AE receiver. This is the continuation of a study concerning the effect of propagation distance on the acquired AE parameters of pure bending [24].

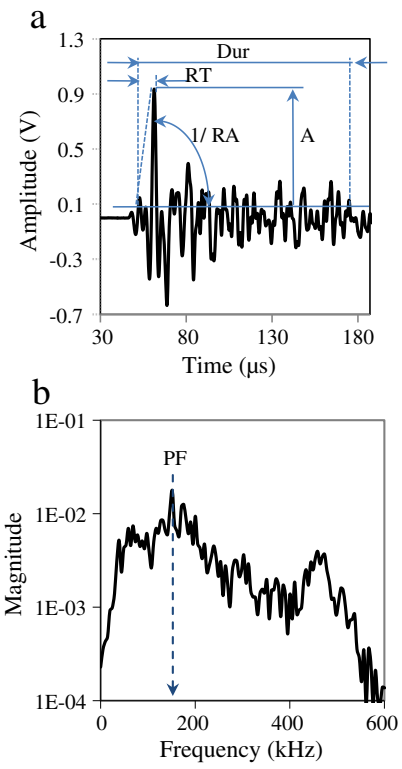

Fig. 1. (a) Typical AE waveform with main parameters, and (b) typical frequency spectrum.

2. Experimental details

2.1. Materials

Two similar mortar mixtures were produced consisting of six specimens each. The specimen size was 40 × 40 × 160 mm as typically used for three-point bending. The aggregates consisted of 100% crushed sand with a maximum aggregate size of 4.75 mm and fineness modulus of 2.93, while the water/cement ratio was 0.55 by mass. The density and the water absorption of the sand were 2500 kg/m^3 and 2.44% respectively. The exact mix proportions were as follows: cement (type II 42.5 N) 440 kg/m^3, water 242 kg/m^3, sand 1529 kg/m^3, and super-plasticizer 4.5 kg/m^3.

Six of the specimens were subjected to three-point bending according to EN 13892-2:2002 [25], see Fig. 2a. A notch was created at the mid span of the bottom (tensile) side in order to secure that the crack would initiate at the center of the specimen. The load was applied at a constant rate of 50 N/s and the loading was automatically

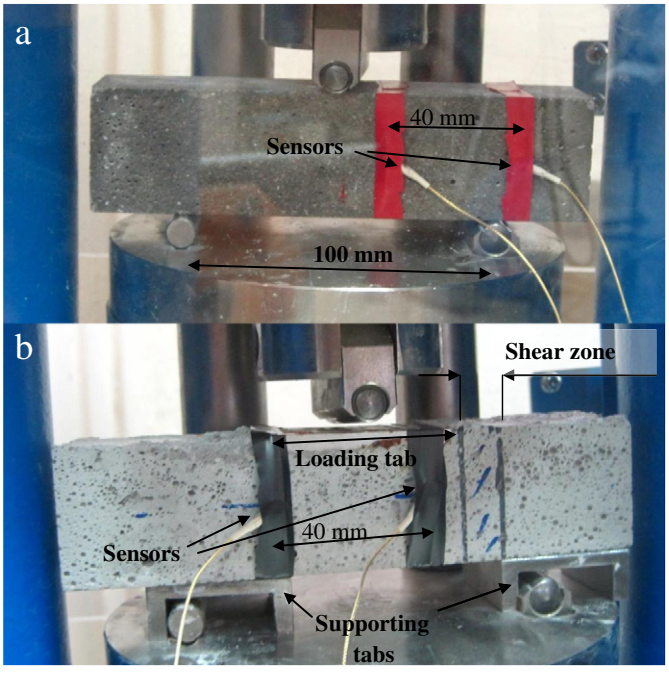

Fig. 2. Experimental setup for (a) three-point bending and (b) shear mode with AE sensors.

terminated at the moment of load drop. A slight modification was done in the molding of the other six specimens that were intended for the study of the shear fracture mode. Specifically, a metal tab with a length of 50 mm and width of 40 mm was placed inside the specimen just after molding at the center of the top side (Fig 2b). This modification of the geometry in combination with the support altered considerably the stress field as will be discussed in a later section.

2.2. Acoustic emission

Concerning AE monitoring, two broadband AE sensors with maximum sensitivity at 500 kHz (Pico, PAC) were attached to the side of the specimen as seen in Fig. 2a and b. Roller bearing grease was used to promote acoustic coupling, while the sensors were secured by tape (see again Fig. 2). The horizontal distance between the sensors was 40 mm and the first was placed at the horizontal distance of 15 mm from the expected location of the crack which was secured by small notches, as seen in Fig. 2a for the bending and in Fig. 2b for the "shear" type. The signals were recorded in a two-channel monitoring board PCI-2, PAC with a sampling rate of 5 MHz. The threshold was set to 40 dB to avoid ambient noise and the acquired signals were pre-amplified by another 40 dB.

3. Fracture details and FEM analysis

As aforementioned, the target of the study was to develop and passively monitor different fracture modes in mortar specimens. In the simple 3-point bending test, it is easily understood that fracture starts from the bottom due to high tensile stresses. However, concerning the modification of the geometry to test a "mixed" fracture mode, simple FEM analysis was deemed necessary. Two dimensional analysis was conducted for both types of testing for comparison purposes. A free version of commercially available software was used [26]. For the three-point bending simulation under discussion, the model geometry was 160×40 mm, similar to the front view of the specimen. Plain strain conditions were applied. The load was placed at the central point of the top side and support was provided by two points at the bottom side (see Fig. 3a) at the exact points as dictated by the experiment. For the slightly modified geometry intended for the shear-driven fracture, again the front view of the specimen was modeled. In this case the load is applied in a distributed area on the top of the specimen due to a metal tab placed when the material was fresh, while the bottom support is also distributed at two areas (see Fig. 4a). The supports were placed in such a way that there is an overlap of opposing forces at the left side (area A in Fig. 4a), while there is a zone of 10 mm without overlapping at the right side between the load and support distributions (area B). The geometry can also be seen in the photograph of Fig. 2b. This free zone (B) in conjunction with a small notch that was created at the end of the support (point C) led in the fracture of the specimen at this zone. Material elastic constants were indicatively assigned the following values: Elastic modulus 20 GPa and Poisson's ratio 0.2 leading to shear modulus of 8.3 GPa. These values are typical for cementitious materials without however being the only possible values. The geometry was divided into triangular elements with a nominal side of 6.5 mm, while the total number of nodes was 163. Other mesh sizes were also tested (element side of 8 mm) and resulted in very similar stress values with

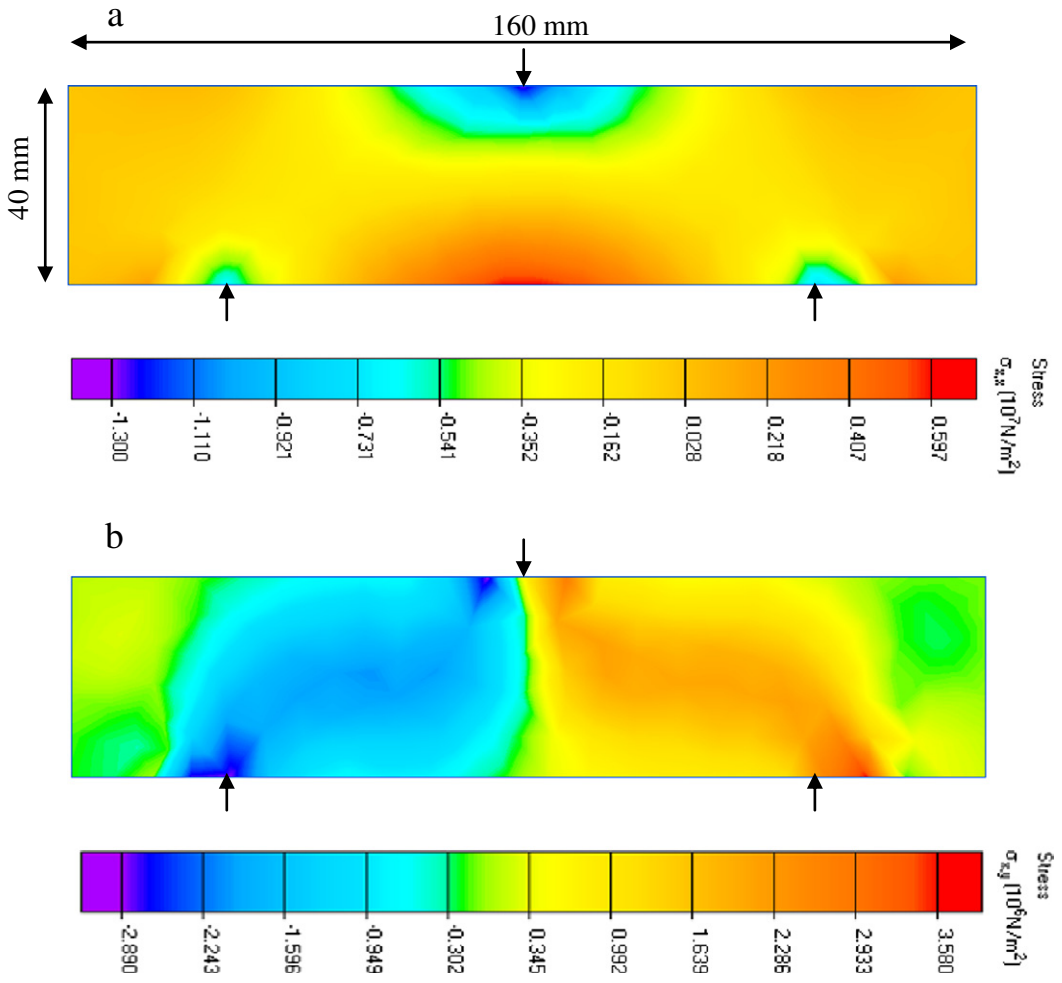

Fig. 3. Stress field for three point bending test: (a) normal stress (σ_{xx}), and (b) shear stress (τ_{xy}).

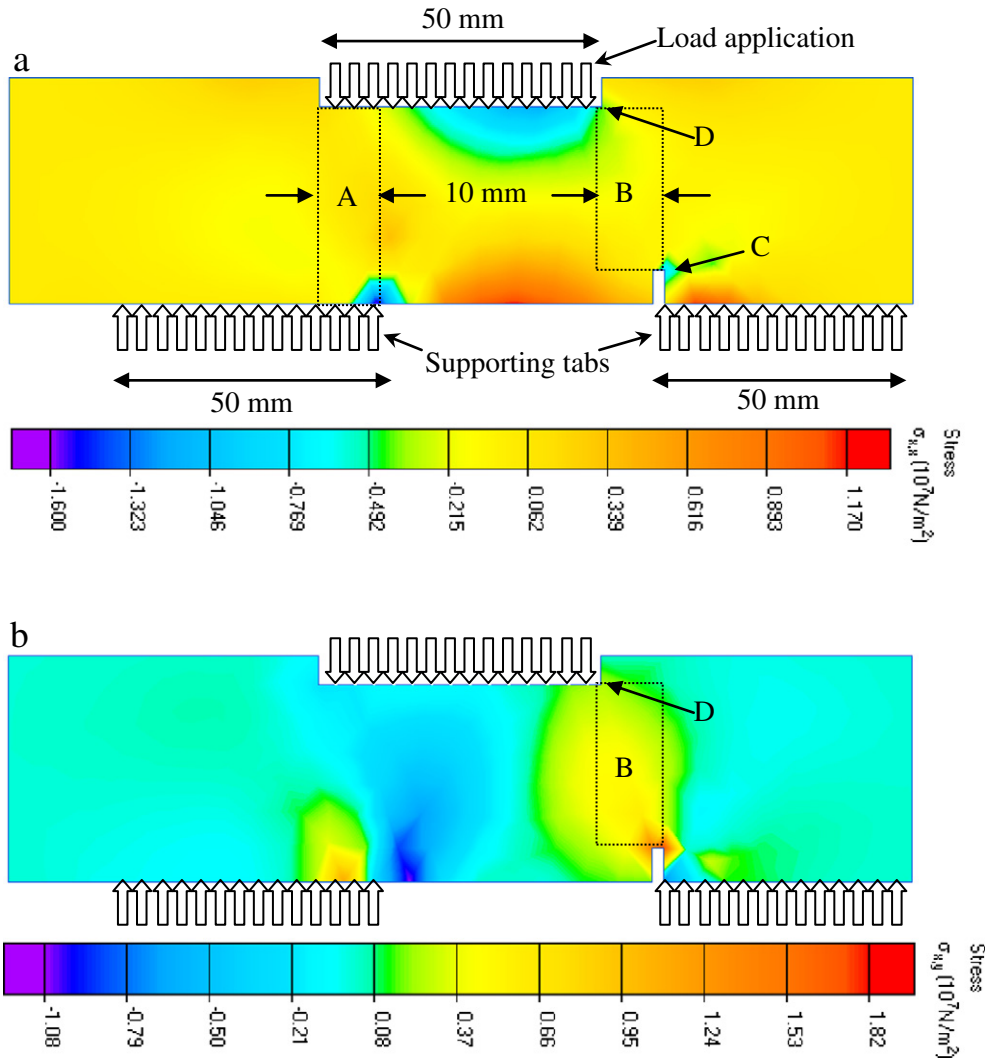

Fig. 4. Stress field for the "shear" test: (a) normal stress (σ_{xx}), and (b) shear stress (τ_{xy}).

the ones discussed below. Results of the analysis concerning normal and shear stresses are seen in Figs. 3 and 4 for the two types of specimens. As expected, the normal stresses in the pure bending case, shown in Fig. 3a, exhibit a positive maximum at the mid span of the bottom, where the specimens actually broke. This happens due to the weak tensile strength of cementitious material. Fig. 3b shows shear stresses with the same loading condition. Maximum shear stresses are of lower level (approximately half of the corresponding normal), while at the mid-span of the specimen shear stresses change sign, being very close to zero. Therefore, the crack at the center of the specimen can be considered quite close to pure tensile mode.

Concerning the specimen intended for more "shear" fracture, corresponding results are seen in Fig. 4a and b. Forces and supports were applied by means of tabs instead of contact points. The load application area on top and the left support were overlapped, while there is no overlap between the load application and the support at the right bottom (area B in Fig. 4a). This led to an unsupported zone available for shearing of the specimen. Fig. 4a and b shows the normal and shear stresses respectively. It is seen that the maximum normal stresses are exhibited away from the notch with the maximum tension near the bottom mid-span point. However, the tip of the notch clearly exhibits maximum shear stresses, as seen in Fig. 4b, while the shear zone extends to the top in a diagonal direction until the normal angle in point D. Although, low normal stresses may still be applied on the same zone, it can be reasonably argued that the initiation and propagation of the specific crack include strong shear components which was not the case for the pure bending experiment. Fig. 5 shows fractured specimens after both types of tests. As the simulation results imply, the specimen tested in pure bending (Fig. 5a) was fractured at the mid span where maximum tension is exhibited in Fig. 3a. For the "shear" type of test (Fig. 5b), the crack extends diagonally from the notch to the top within the zone shear stresses indicated by FEM and being in agreement with the simulation results. Since the cracking events include different constituents of the stress tensor, monitoring by AE is expected to show distinct trends, something presented and analyzed in the following section.

4. AE results

Results of the acoustic monitoring concern the total activity and the qualitative features of the waveforms. Fig. 6a shows the accumulated AE signals (hits) received by the near-by sensors (15 mm from the crack) for typical bending and shear tests. For both of them the population of hits is built gradually until the moment of final failure where the maximum hit rate is exhibited. The total number of signals is limited below 100 hits. The 2nd sensor (55 mm away from the crack) follows the same behavior with the difference of slightly lower number of hits (Fig. 6b). This is reasonable due to longer propagation distance which crucially attenuates some of the signals already captured by the 1st receiver, below the threshold level.

Fig. 5. Fractured specimens after (a) bending, and (b) shear.

Fig. 7a shows the RA of the signals received by the 1st sensor for the same experiments. Concerning the bending mode, RA ranges mainly below 1 ms/V except for the moment of final failure when some RA values of more than 10 ms/V are noted. The specimen under shear on the other hand exhibited some RA values of level higher than 1 ms/V, while at the end it showed a certain increase similar or even higher than the bending case. The solid lines are the moving average of the recent five values in order to show the trends in a more clear way. The corresponding RA values as captured by the 2nd sensor are seen in Fig. 7b. Again the signals coming from the shear experiment exhibit generally higher RA values, as revealed by the moving average lines.

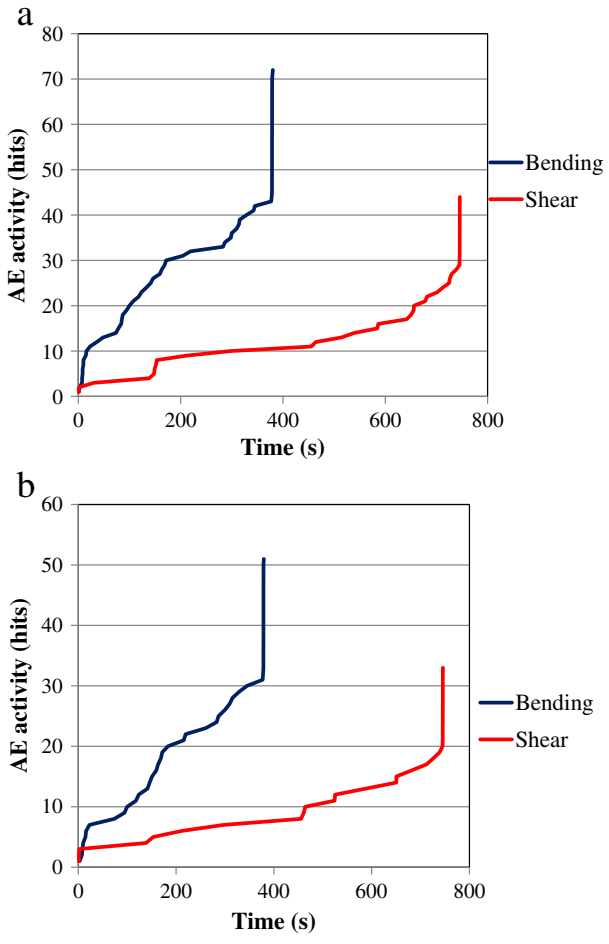

Fig. 6. Cumulative AE activity of typical tests: (a) 1st sensor (15 mm from the crack), and (b) 2nd sensor (55 mm from the crack).

Typical results concerning the AF are included in Fig. 8a and b for both fracture modes and sensors. In this case, the bending type of fracture exhibits higher frequency in average, ranging from 50 kHz to 400 kHz while at failure AF values close to zero are also noted. On the other hand shear mode results in frequencies up to 250 kHz, while at macro-fracture they are limited below 150 kHz. AF measured by the 2nd sensor follows similar trends with the shear being again notably lower than bending (Fig. 8b). These results are some typical comparisons between pairs of specimens while in the next paragraph the average values of all specimens are discussed.

In the present case, the ambient noise level was low and the applied threshold secured that no external signals are acquired. In order to increase the reliability of the obtained information even more, the following analysis concerns only the “AE events”. This means that for any hit of the first sensor analyzed, another hit was also recorded by the second sensor which belonged to the same source event. Typically for each experiment a number of approximately 20 events were recorded. The AF and RA value of these events are averaged and presented in Fig. 9. Tensile fracture mode specimens monitored by the 1st sensor, typically exhibit AF between 110 kHz and 160 kHz, while their RA is less than 500 μs/V in average. Fig. 9 contains also the corresponding values for the shear type of testing. The average values of AF of the five specimens as measured by the 1st sensor show a maximum AF of 105 kHz and a minimum RA of 840 μs/V being totally separated from the corresponding population of the bending (tensile) mode as monitored by the sensor at the same distance.

Concerning the same events monitored by the 2nd sensor (at 55 mm) distinct changes are shown. Tensile events exhibit lower frequency (from 80 kHz to 140 kHz) and higher RA, close to 1000 μs/V, compared to the sensor at 15 mm. This is an indication of waveform distortion that occurs in heterogeneous media like cement mortar.

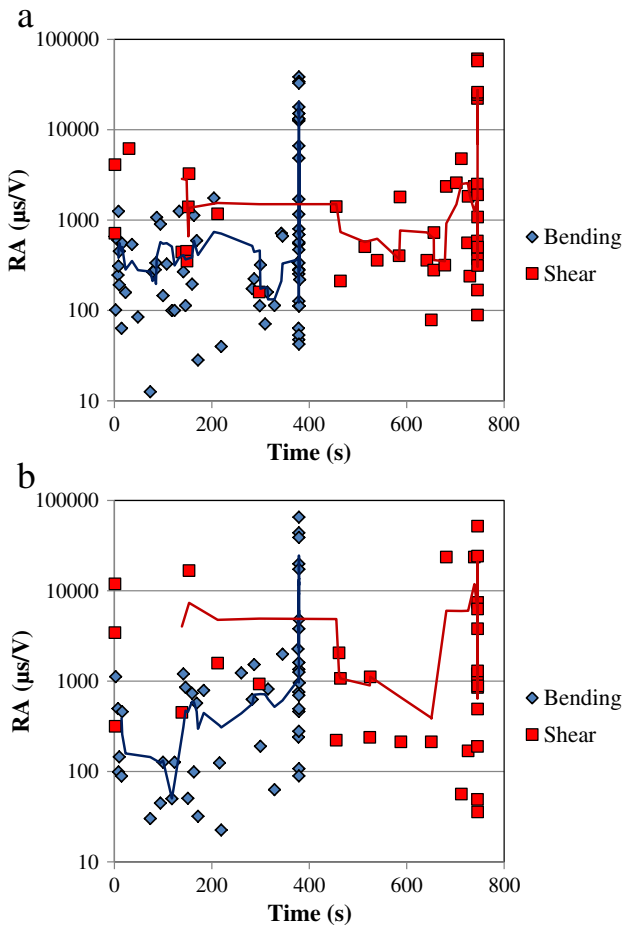

Fig. 7. RA vs. time for different fracture modes as monitored by: (a) 1st sensor (15 mm from the crack), (b) 2nd sensor (55 mm from the crack).

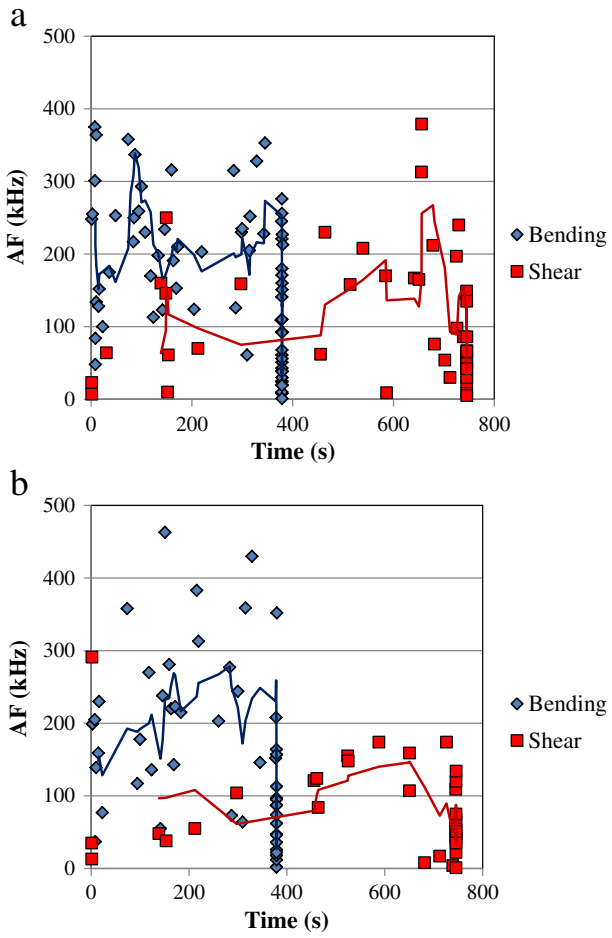

Fig. 8. AF vs. time for different fracture modes as monitored by: (a) 1st sensor (15 mm from the crack), (b) 2nd sensor (55 mm from the crack).

Scattering on the boundaries of the microstructure (sand grains, air bubbles) reduces the representative frequency, mainly by more effectively attenuating higher components, while it also elongates the pulse because the energy is redistributed to many random wave paths after each impact and does not arrive in a straight line as would happen in a homogeneous medium [27,28]. Additionally, the sensor at 55 mm exhibits much lower frequency (around 60 kHz) and higher RA values (2000 to 5500 μs/V) than the 1st for the shear mode as well. These indications show that any AE study should be combined with knowledge of wave propagation in the specific material, since a few centimeters of additional propagation between sensor 1 and 2 force noticeable changes.

The above mentioned AE descriptors (AF and RA) are two of the most powerful in discriminating damage mode [1,4,17]. However, the individual fracture modes result in differences in other AE parameters as well. Fig. 10 shows the average values of peak frequency (PF) and Amplitude (Amp) for both modes and sensor distances. The tensile mode exhibits higher amplitude and peak frequency than shear in average for the same sensor distances. Apart from the effect of fracturing mode, the effect of distance is again highlighted since the sensor at 55 mm obtains much lower amplitude and peak frequencies than the near-by sensor for both cracking modes.

Table 1 summarizes the average values of basic AE parameters for the two examined fracture modes and propagation distances. One conclusion from these data concerns the discrepancies in the AE descriptors between the different fracture modes monitored at a standard distance. Shear (or mixed mode) fracture emits signals of lower basic frequency characteristics and amplitude but longer in rise time than tensile. The differences are visible in all parameters but greater changes are seen in RA, for which the values of shear (1734 μs/V) are more than six times higher than those of tension (278 μs/V). The decrease in amplitude is also large since shear emissions are lower than tensile by almost 5 dB (58.4 dB to 53.8 dB). Additionally, frequency characteristics measured either by the AF or the PF show strong decrease for the shear mode by about 35% compared to tensile events. Overall, the clearly separated averages and the relatively limited variance (presented as standard deviation over average,

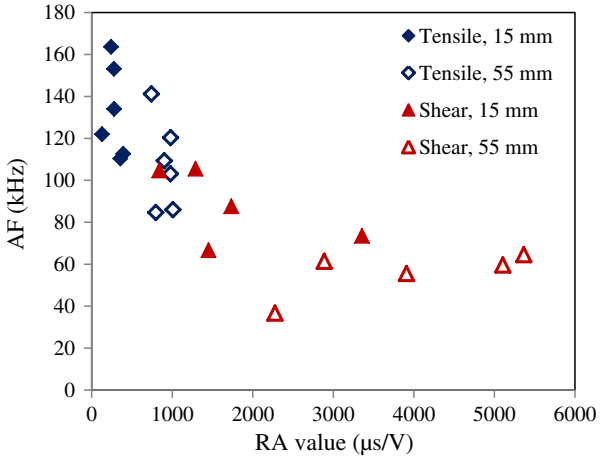

Fig. 9. AF vs. RA value for different fracture modes and sensor distances (each symbol is the average of all AE events of each experiment).

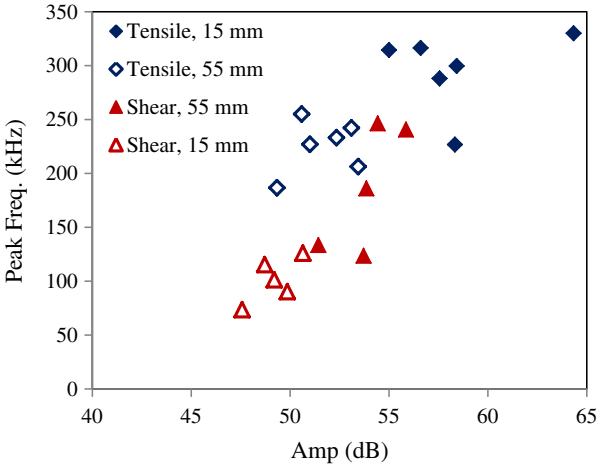

Fig. 10. PF vs. Amp for different fracture modes and sensor distances (each symbol is the average of all AE events of each experiment).

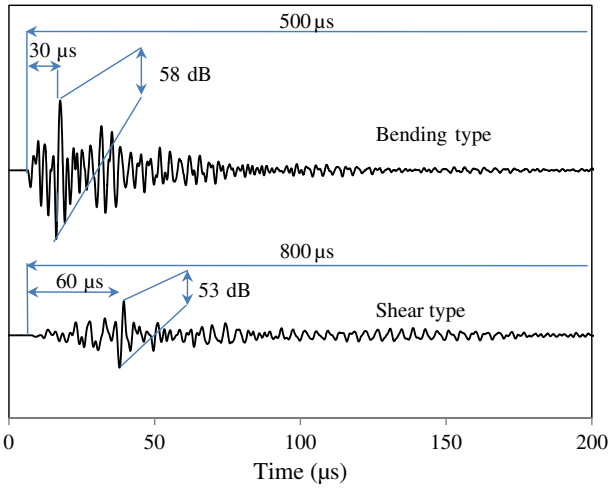

Fig. 11. Typical waveforms attributed to different fracture modes (distance 15 mm).

coefficient of variation, COV) enable quite good separation of the clusters without the need to employ pattern recognition approaches. It is seen therefore, that in simple geometries in laboratory conditions, the cracking mode can be reliably monitored by its AE fingerprint.

However, the differences measured by the two sensors show how much the results are dependent on the testing conditions and specifically the distance between the cracks and the sensors. The additional distance of 40 mm between the two sensors forces a decrease of more than 20% in frequency parameters (132 kHz to 109 kHz for tension and 87 kHz to 56 kHz for shear) and an increase by three to four times in RA (278 μs/V to 900 μs/V for tensile and 1734 μs/V to 3908 μs/V for shear). Indeed, scattering is quite strong in this kind of material due to inhomogeneity which distorts the shape of the propagating pulse resulting also in considerable attenuation especially at the higher frequencies. Complimentary to scattering, viscous damping of the material contributes to loss of transmitted energy to heat, resulting in a decrease in amplitude of 5 to 6 dB between the first and the second receiver.

5. Discussion

Combining the information of Table 1, an illustration of an AE waveform typical of each mode, as recorded by the sensor at 15 mm is shown in Fig. 11. The "tensile" waveform has an amplitude much higher than shear, while it is also characterized by shorter "rise time" (30 μs compared to 60 μs). Additionally the total duration of a tensile signal is significantly shorter than shear.

The above mentioned results show that the separation of fracture modes is tangible in laboratory conditions. The characterization in real structures would also be tangible if it weren't for the signal distortion and attenuation that occur in heterogeneous materials. Along with the sensor's response this is another parameter that renders the application

Table 1
Basic AE parameters for different modes and propagation distances to the sensor.

Mode and distance		AF (kHz)	RA (μs/V)	AMP (dB)	P-Freq (kHz)
Tensile (15 mm)	Average	132.4	278.4	58.4	295.2
	COV	16.5%	33.2%	5.5%	12.5%
Shear (15 mm)	Average	87.6	1733.6	53.8	186.1
	COV	18.0%	49.7%	2.7%	27.7%
Tensile (55 mm)	Average	109.3	900.7	52.3	233.2
	COV	19.6%	12.2%	3.0%	10.5%
Shear (55 mm)	Average	55.6	3908.0	49.2	101.3
	COV	17.8%	30.8%	2.1%	18.2%

of AE case-specific and does not allow fully exploiting its potential in real structures [29]. If distortion is not taken into account, tensile signals monitored at longer distance (55 mm) may well be overlapped with shear signals received at 15 mm from the source, see Figs. 9 and 10. This would prevent from applying characterization in real structures where the distances between cracks and sensors are typically of the order of meters and highlights the importance of incorporating the distance that the wave traveled from the crack tip to the sensor. Fortunately contemporary AE equipment includes software with powerful location algorithms. Therefore, the time delay between acquisition of waveforms of the same event at different positions leads to calculation of the crack location in real time. This enables an inverse procedure for evaluation of the signal as-emitted by the crack before distortion due to inhomogeneity or geometry is accumulated in the as-received by the sensor waveform [16].

Another issue that should be highlighted concerning the specific study is that although cement mortar can be regarded as macroscopically homogeneous concerning the stress analysis, still the material contains grains with an average size of 2 mm. Therefore, it is reasonable that the crack propagates on the interphase between the matrix and the inclusions and the macroscopically simulated or expected stress fields may somehow differ from the actual in the micro-scale of the grain–matrix interphase. If the material was totally homogeneous then the actual stresses would possibly be closer to the stresses simulated. However, this study is focused on cementitious materials, which in any case include sand grains and therefore, this is a realistic way to study modes of fracture in cement-based materials. As a future task experiments on marble specimens are scheduled. Also possible modifications in the geometry will be studied in order to develop pure shear fracture, since currently low level normal stresses are also developed on the tip of the notch. Upgrading the scale of the problem is also being considered in order to facilitate concrete testing.

Finally, the sensor response function should be discussed. The results obtained refer to a specific sensor type. This type may be considered a broadband compared to other resonant AE sensors but still its response is far from being flat. Therefore, the waveforms captured are certainly influenced by the sensor "preferences". The specific values obtained would definitely differ if other pairs of sensors had been used in the experiment. However, what is emphasized herein is the change between the emissions of the different fracture modes and separation distances. All the experiments were conducted by the same pair of sensors so that any distinct trends are attributed directly to the fracture mode and separation distance. In any case, in the field of concrete AE, standardization is currently being attempted [17] meaning for the proposed type of sensor a similar procedure could

be undertaken to establish a database with the AE fingerprints of fracture modes at various propagation distances.

6. Conclusions

The present paper occupies with passive monitoring of the fracture process in cementitious materials with the use of the acoustic emission technique. The main aim is to characterize the acoustic signature of fracture modes. For this reason, tensile and shear fracture modes were targeted. Both types of experiments were conducted on the same loading equipment with slight modifications. Elementary finite element analysis showed that the modifications were actually effective to alter the stress field and shift from the normal tensile stresses (responsible for fracture in three point bending) to dominant shear. Monitoring with broadband AE sensors revealed distinct trends for the different fracture modes. Specifically AE signals from tensile tests exhibit higher amplitude and frequency, while those from shear tests exhibit longer duration and lower rising angle, as measured by the RA value. The results show that accurate characterization of modes is possible in laboratory conditions based on simple features recorded by one AE sensor. This would be very beneficial for warning against final failure since cracking modes generally follow a sequence during fracture. Results also highlight the need to jointly study AE with elastic wave propagation since an additional distance of a few centimeters alters significantly the frequency content and shape of the acquired waveforms. This is an important parameter that needs to be amended in order to fully exploit the capabilities of AE in laboratory conditions and expand reliable characterization in real structures.

Acknowledgment

The contribution of Dipl. Materials Engineer Pelia Giannoulatou in making and testing the mortar specimens is acknowledged.

This research project has been co-financed by the European Union (European Regional Development Fund — ERDF) and Greek National Funds through the Operational Program "THESSALY MAINLAND GREECE AND EPIRUS-2007-2013" of the National Strategic Reference Framework (NSRF 2007–2013).

References

[1] K. Ohno, M. Ohtsu, Crack classification in concrete based on acoustic emission, Constr. Build. Mater. 24 (12) (2010) 2339–2346.
[2] D.G. Aggelis, T. Shiotani, S. Momoki, A. Hirama, Acoustic emission and ultrasound for damage characterization of concrete elements, ACI Mater. J. 106 (6) (2009) 509–514.
[3] D.G. Aggelis, D.V. Soulioti, N.M. Barkoula, A.S. Paipetis, T.E. Matikas, Influence of fiber chemical coating on the acoustic emission behavior of steel fiber reinforced concrete, Cem. Concr. Compos. 34 (2012) 62–67.
[4] D.G. Aggelis, Classification of cracking mode in concrete by acoustic emission parameters, Mech. Res. Commun. 38 (2011) 153–157.
[5] C.U. Grosse, F. Finck, Quantitative evaluation of fracture processes in concrete using signal-based acoustic emission techniques, Cem. Concr. Compos. 28 (2006) 330–336.
[6] M. Shigeishi, M. Ohtsu, Acoustic emission moment tensor analysis: development for crack identification in concrete materials, Constr. Build. Mater. 15 (2001) 311–319.
[7] T. Shiotani, Evaluation of long-term stability for rock slope by means of acoustic emission technique, NDT&E Int. 39 (3) (2006) 217–228.
[8] T. Shiotani, D.G. Aggelis, O. Makishima, Global monitoring of large concrete structures using acoustic emission and ultrasonic techniques, J. Bridg. Eng.-ASCE 14 (3) (2009) 188–192.
[9] C.U. Grosse, M. Ohtsu, Acoustic Emission Testing, Springer, Heidelberg, 2008.
[10] A. Carpinteri, F. Cardone, G. Lacidogna, Energy emissions from failure phenomena: mechanical, electromagnetic, nuclear, Exp. Mech. 50 (2010) 1235–1243.
[11] B.-K. Jang, T. Kishi, Mechanical properties of TiNi fiber impregnated CFRP composites, Mater. Lett. 60 (2006) 518–521.
[12] H. Elaqra, N. Godin, G. Peix, M. R'Mili, G. Fantozzi, Damage evolution analysis in mortar, during compressive loading using acoustic emission and X-ray tomography: effects of the sand/cement ratio, Cem. Concr. Res. 37 (2007) 703–713.
[13] M. Ohtsu, H. Watanabe, Quantitative damage estimation of concrete by acoustic emission, Constr. Build. Mater. 15 (2001) 217–224.
[14] D. Soulioti, N.M. Barkoula, A. Paipetis, T.E. Matikas, T. Shiotani, D.G. Aggelis, Acoustic emission behavior of steel fibre reinforced concrete under bending, Constr. Build. Mater. 23 (2009) 3532–3536.
[15] Y. Lu, Z. Li, W.I. Liao, Damage monitoring of reinforced concrete frames under seismic loading using cement-based piezoelectric sensor, Mater. Struct. 44 (7) (2011) 1273–1285.
[16] D.G. Aggelis, T.E. Matikas, Effect of plate wave dispersion on the acoustic emission parameters in metals, Comput. Struct. 98–99 (2012) 17–22.
[17] M. Ohtsu, Recommendations of RILEM Technical Committee 212-ACD: acoustic emission and related NDE techniques for crack detection and damage evaluation in concrete: 3. Test method for classification of active cracks in concrete structures by acoustic emission, Mater. Struct. 43 (9) (2010) 1187–1189.
[18] K. Van Tittelboom, N. De Belie, F. Lehmann, C.U. Grosse, Acoustic emission analysis for the quantification of autonomous crack healing in concrete, Constr. Build. Mater. 28 (2012) 333–341.
[19] S. Granger, A. Loukili, G. Pijaudier-Cabot, G. Chanvillard, Experimental characterization of the self-healing of cracks in an ultra high performance cementitious material: mechanical tests and acoustic emission analysis, Cem. Concr. Res. 37 (2007) 519–527.
[20] M.M. Kuba, D.C. Van Aken, Plastic strain accommodation and acoustic emission during melting of embedded particles, Mater. Lett. 77 (2012) 89–92.
[21] K. Wu, B. Chen, W. Yao, Study of the influence of aggregate size distribution on mechanical properties of concrete by acoustic emission technique, Cem. Concr. Res. 31 (2001) 919–923.
[22] T.P. Philippidis, V.N. Nikolaidis, A.A. Anastassopoulos, Damage characterization of carbon/carbon laminates using neural network techniques on AE signals, NDT&E Int. 31 (5) (1998) 329–340.
[23] D.G. Aggelis, N.M. Barkoula, T.E. Matikas, A.S. Paipetis, Acoustic emission monitoring of degradation of cross ply laminates, J. Acoust. Soc. Am. 127 (6) (2010) EL246–EL251.
[24] D.G. Aggelis, A.C. Mpalaskas, D. Ntalakas, T.E. Matikas, Effect of wave distortion on acoustic emission characterization of cementitious materials, Constr. Build. Mater. 35 (2012) 183–190.
[25] EN 13892-2:2002, Methods of Test for Screed Materials — Part 2: Determination of Flexural and Compressive Strength, 2002.
[26] http://www.quickfield.com/, (Students' QuickField 5.9).
[27] M.L. Cowan, K. Beaty, J.H. Page, L. Zhengyou, P. Sheng, Group velocity of acoustic waves in strongly scattering media: dependence on the volume fraction of scatterers, Phys. Rev. E 58 (5) (1998) 6626–6636.
[28] D.G. Aggelis, T. Shiotani, Experimental study of surface wave propagation in strongly heterogeneous media, J. Acoust. Soc. Am. 122 (5) (2007) 151–157, (EL).
[29] J.J. Scholey, P.D. Wilcox, M.R. Wisnom, M.I. Friswell, Quantitative experimental measurements of matrix cracking and delamination using acoustic emission, Compos. Anal. 41 (2010) 612–623.